J Mater Sci: Mater Electron (2015) 26:8432–8441
DOI 10.1007/s10854-015-3512-3

Stable piezoelectric property of modified $BiFeO_3$–$BaTiO_3$ lead-free piezoceramics

Yang Lin[1] · Linlin Zhang[1] · Jian Yu[1]

Received: 3 May 2015 / Accepted: 17 July 2015 / Published online: 24 July 2015

Abstract Perovskite-structured $0.696BiFeO_3$–$0.014Bi(Zn_{1/2}Ti_{1/2})O_3$–$0.29BaTiO_3$ (BF69.6–BZT1.4–BT29) lead-free piezoceramics with various MnO_2 addition were prepared using a refined solid state reaction electroceramic processing. Powder X-ray diffraction measurements showed their crystallographic structure being of rhombohedral structure and scanning electron microscopy observations revealed that MnO_2-doping enhances ceramic microstructure grain size growth. In contrast to BF–BT ceramics, low dielectric loss ceramics were obtained with combined strategies of refined electroceramic processing, Mn-doping and adding BZT third member. A good combination of ferroelectric and piezoelectric property was obtained in the 0.22 and 0.26 % in weight MnO_2-doped BF69.6–BZT1.4–BT29 coarse-grained ceramics and discussed in relation to microstructure grain size effect and point defect effect. Excellent time and thermal aging stabilities of piezoelectric constant d_{33} were also experimentally demonstrated and argued resulting from the feature of higher ferroelectric Curie temperature (T_C) and no ferroelectric–ferroelectric structural phase transition below T_C of BF–BZT–BT system.

1 Introduction

Piezoceramics are one of most important functional materials, which have been widely used to transform electrical signals into mechanical strain and vice versa in electromechanical systems as both sensors and actuators [1]. On one hand, environmental concerns are strongly driving the developments of lead-free piezoceramics. As the state-of-art review articles discussed [2–4], compositional engineering approaches to achieve enhanced piezoelectric properties in lead-free materials are being focused on $K_{1-x}Na_xNbO_3$, $(1-x)(Bi_{0.5}(Na,K)_{0.5})TiO_3$–$xBaTiO_3$, $(1-x)Ba(Zr_{0.2}Ti_{0.8})O_3$–$x(Ba_{0.7}Ca_{0.3})TiO_3$, and $BiFeO_3$–$ATiO_3$(A = Ba, Sr, Ca, $Bi_{0.5}Na_{0.5}$, and $Bi_{0.5}K_{0.5}$) solid solutions. Structural engineering approaches focus on extending structural phase boundary and optimizing microstructure grain size, grain orientation or texture to induce large piezoelectric properties in lead-free piezoceramics. As promising candidates for lead-free materials, $(K,Na)NbO_3$ [5], $(Bi_{0.5}(Na,K)_{0.5})TiO_3$–$BaTiO_3$ [6], and $Ba(Zr_{0.2}Ti_{0.8})O_3$–$(Ba_{0.7}Ca_{0.3})TiO_3$ [7–9] have been intensively studied and exhibit good piezoelectricity. However, due to low depolarization/Curie temperature, these lead-free ceramics exhibit a poor temperature stability of piezoelectric properties [2–9]. On the other hand, novel piezoceramics with higher ferroelectric Curie temperature (T_C) and no ferroelectric–ferroelectric (FE–FE) phase transition below T_C are required for good stability of piezoelectric performances, particularly in those high temperature application fields such as automotive fuel injection, oil logging and aerospace accelerometer [10–16].

$BiFeO_3$ is in a rhombohedrally distorted perovskite structure (space group *R3c*) at room temperature and undergoes a ferroelectric–paraelectric phase transition at T_C = 830 °C. Perovskite $BiFeO_3$ and $BaTiO_3$ has been demonstrated to form continuous solid solution of (1−x)BF–xBT with tetragonal (x = 0.92–1), pseudocubic (x = 0.33–0.92), and rhombohedral (x = 0–0.33) [17–19]. As alternative to current lead-free materials, BF–BT solid solution is a potential lead-free piezoceramics, which

✉ Jian Yu
jyu@tongji.edu.cn

[1] Functional Materials Research Laboratory and Key Laboratory of Advanced Civil Engineering Materials (Ministry of Education), School of Materials Science and Engineering, Tongji University, Shanghai 201800, China

combines both compositional and structural engineering approaches with T_C more than 500 °C to realize higher piezoelectric properties and temperature stability. Nevertheless, poor perovskite phase stability and low high-field electrical resistivity led to difficulty in observing ferroelectric polarization switching in $BiFeO_3$ [20, 21]. Similarly, electrical characterizations of BF–BT ceramics have also been complicated by high dielectric losses and high conductivity, and ferroelectric polarization switching measurements often revealed them be of a lossy dielectric [17, 18]. To improve DC resistivity and reduce low-frequency AC loss is required in practice to enable high field poling and characterization of piezoelectric properties in the BF and BF–BT systems.

Utilizing MnO_2 modification and optimized solid state sintering conditions, Leontsev and Eitel found that BF–BT ceramics can be poled and show measurable piezoelectric coefficients in the compositional range of x = 0.22–0.40. For 0.1 wt% MnO_2-doped 0.67BF–0.33BT (0.75BF–0.25BT) ceramics, a piezoelectric property of $d_{33} = 70$ (116) pC/N, $\varepsilon_r = 750$ (557), $\tan\delta = 0.068$ (0.046), and $T_C = 605$ °C (619 °C) was reported [22, 23]. While, a maximum piezoelectric property of $d_{33} = 124$ pC/N, $\varepsilon_{33}^T/\varepsilon_0 = 760$, $\tan\delta = 0.078$, and $k_p = 0.29$ was reported at optimum composition of 0.725BF–0.275BT, i.e., at structural phase boundary between rhombohedral and pseudocubic [24]. Till now, extensive studies have reported different composition of structural phase boundary between rhombohedral and pseudocubic of x = 0.275, [24] x = 0.33 [17, 18] or over the range of x = 0.25–0.33 [22, 23]. It is of interest to note that, even though Mn-doping strategy is effective to decrease dielectric loss, dielectric loss of BF–BT ceramics reported so far is still far away from practical level of $\tan\delta \leq 0.02$.

The thermodynamic stability of $BiFeO_3$ and volatility of Bi were often thought as main causes for lattice vacancies and consequently makes poling treatment difficult to set full piezoelectricity. To improve thermodynamic stability of $BiFeO_3$, our recent experiments demonstrated that forming a ternary solid solution is a more effective approach to fabricate robust insulating phase-pure $BiFeO_3$-based ceramics than forming a binary solid solution [25–27]. Rhombohedral $Bi_{1-x}La_xFe_{1-y}Ti_yO_3$ ceramics with $0.02 \leq x \leq 0.12$ and $0.01 \leq y \leq 0.08$, prepared using a refined solid-state reaction electroceramic processing with sintering temperature at 890 °C , exhibit robust insulating properties with resistivity on the order of $10^{11}\Omega$m under an electric field of 80 kV/cm and dielectric loss below 0.02 at frequency of 1 kHz. Contemporarily, high-temperature X-ray diffraction (XRD) measurements detected no peritectic decomposition of $Bi_{1-x}La_xFe_{1-y}Ti_yO_3$ up to 850 °C, which implies these ceramics are more thermodynamically stable than $BiFeO_3$ and singly substituted $BiFeO_3$ [27]. At the same time, various Bi-perovskites (e.g. $Bi(Zn_{1/2}Ti_{1/2})O_3$ [28–30], $Bi(Mg_{1/2}Ti_{1/2})O_3$ [31–33], $Bi(Ni_{1/2}Ti_{1/2})O_3$ [34], etc.) have been added into BF–BT system to improve insulating and decrease dielectric loss. Combined with Mn-doping strategy, $\tan\delta \sim 0.045$ was reported for the 1 mol% MnO_2-doped $(0.70-x)$BF–xBZT–0.30BT ceramics with x = 0−0.15 sintered at 960 °C for 2 h [28]. And $\tan\delta = 0.034$ was reported for 0.3 wt% MnO_2-doped $0.69BiFeO_3$–$0.02Bi(Mg_{1/2}Ti_{1/2})O_3$–$0.29BaTiO_3$ ceramics sintered at 900 °C for 10 h [33]. In contrast to $(K,Na)NbO_3$, $(Bi_{0.5}(Na,K)_{0.5})TiO_3$–$BaTiO_3$ and $Ba(Zr_{0.2}Ti_{0.8})O_3$–$(Ba_{0.7}Ca_{0.3})TiO_3$, good thermal aging stability of piezoelectric properties was reported for Mn-doped BF–BMT–BT and BF–BZT–BT lead-free ceramics [29, 33]. Nevertheless, consistent structural, dielectric and piezoelectric data are absent yet for Mn-doped BF–BZT–BT piezoceramics [28, 29].

In this paper, $0.696BiFeO_3$–$0.014Bi(Zn_{1/2}Ti_{1/2})O_3$–$0.29BaTiO_3$ (labelled as BF69.6–BZT1.4–BT29) composition with various MnO_2 dopant amount was chosen as typical model to systematically and consistently investigate composition effect on crystallographic structure, microstructure, dielectric, ferroelectric, and piezoelectric properties of modified BF–BT lead-free piezoceramics. BF69.6–BZT1.4–BT29 composition is situated around the middle of those reported critical values for the composition-structural phase boundary between rhombohedral and pseudocubic phase. A maximum piezoresponse was achieved here for optimized Mn-doped BF69.6–BZT1.4–BT29 ceramics, while excellent time and thermal aging stabilities of piezoelectric constant was demonstrated experimentally and discussed in relation to its higher T_C and no FE–FE phase transition below T_C in BF–BZT–BT system.

2 Experimental procedure

Pure and MnO_2-doped BF69.6–BZT1.4–BT29 ceramics were prepared by traditional solid state reaction method with Bi_2O_3 (99 %, Alfa Aesar), Fe_2O_3 (99.945 %, Alfa Aesar), $BaCO_3$ (99.8 %, Alfa Aesar), TiO_2 (99.9 %, Alfa Aesar), ZnO (99.5 %, Acros), and MnO_2 (99.9 %, Alfa Aesar) as raw materials. Stoichiometric mixtures of raw oxides were ground in corundum mortar with ethanol for 2 h and then calcined at 700 °C for 5 h. In order to protect off-stoichiometry due to Bi_2O_3 adhering on mortar, surfactants were added into mixture before grinding [25–27]. The partial reacted mixed powders were further ground and calcined at 780 °C for 5 h. After calcination, powders were reground, granulated with PVA binder, and pressed uniaxially into green pellets under 250 MPa. The pellets were de-bindered at 600 °C for 2 h and sintered at 900 °C for 10 h (if not obviously pointed out) in a closed alumina crucible of air atmosphere, then cooling with oven.

XRD was used to characterize their crystallographic structure. Microstructure of ceramic fracture surface was observed using scanning electron microscopy (SEM). For electrical characterization, the ceramic pellets were polished, coated with silver paste (Xi'an Hongxing) and fired at 600 °C for 10 min. The frequency- and temperature-dependent dielectric properties were measured using Agilent precision LCR meter. The polarization versus electric field (P–E) hysteresis loop measurements were carried out with Radiant premier II precision material analyzer in silicone oil. The ceramic poling was carried out in silicone oil at 120 °C under DC electric field of 8 kV/mm for 15 min. After aging 24 h, piezoelectric constant and electromechanical coupling factors were measured with quasi-static piezoelectric d_{33} meter (Institute of Acoustics, Chinese Academy of Sciences ZJ-6A) and Wayne Kerr impedance analyzer, respectively.

3 Results and discussion

3.1 Structural characterizations

For the pure and 0.26 wt% MnO_2-doped BF69.6–BZT1.4–BT29 powders crushed from ceramic pellets sintered at 900 °C for 10 h, XRD measurements were carried out at room temperature and the obtained patterns of the first-order diffraction peaks over range of 10°–40° presented in Fig. 1. It was seen from Fig. 1 that XRD diffraction peaks at 32° and 39° are much asymmetric for the pure sample while they are obviously splitting for the 0.26 % MnO_2-doped sample. Through fitting in origin software as showed in Fig. 1, XRD diffraction peaks at 32° and 39° were fitted

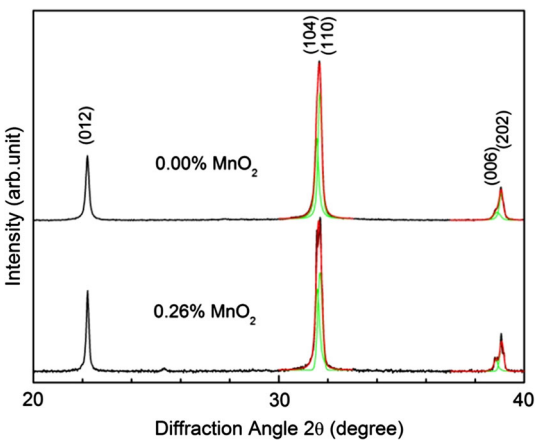

Fig. 1 Powder XRD patterns recorded at room temperature for pure and 0.26 % in weight MnO_2-doped BF69.6–BZT1.4–BT29 ceramics sintered at 900 °C for 10 h. The *red*/*green* [on-line] lines stand for Voigt-shape analyses in Origin software. (hkl) is Miller indices in accordance with rhombohedral $BiFeO_3$ of space group *R3c*

well with two Voigt-shaped peaks for both samples. Referring to $BiFeO_3$ in rhombohedral structure and structural evolution in the BF–BT binary solid solution [17–24], it is concluded that both pure and 0.26 wt% MnO_2-doped BF69.6–BZT1.4–BT29 samples are crystallized in rhombohedral perovskite structure, of which the splitting degree of the diffraction peaks around 39° are closely associated with rhombohedral distortion degree. Meanwhile, no secondary phases of $Bi_{25}FeO_{39}$ and $Bi_2Fe_4O_9$ often met in the $BiFeO_3$-based systems were detected out, which implies that BZT diffuses into BF–BT lattice and single perovskite-type phase is obtained here, in agreement with previous observations [28–30].

SEM measurements on fracture surface of the pure, 0.20, 0.22 and 0.26 wt% MnO_2-doped BF69.6–BZT1.4–BT29 ceramics sintered at 900 °C for 10 h were presented in Fig. 2. It was observed from Fig. 2 that there occurred some residual pores and average grain size was about 1.5 μm in the pure and 0.20 wt% MnO_2-doped samples. When doping MnO_2 was more than 0.20 % in weight, ceramic microstructure grain growth and densification were enhanced in the 0.22 and 0.26 wt% MnO_2-doped BF69.6–BZT1.4–BT29 ceramics. Averaged grain size of 2.2 and 3.6 μm was obtained, respectively, for the 0.22 and 0.26 wt% MnO_2-doped samples sintered at 900 °C for 10 h. At the same time, wide grain size distribution was also observed with increasing MnO_2 addition more than 0.20 wt%. On microstructure grain growth enhanced by Mn-doping, it has been widely observed in the perovkite systems including $0.7BiFeO_3$–$0.3BaTiO_3$ and $Pb(Zr,Ti)O_3$-based ceramics [35–37].

Previously, similar compositions of 1 mol% MnO_2-doped BF67.5–BZT2.5–BT30 [28] and 0.6 wt% MnO_2-doped BF69.58–BZT1.42–BT29 [29] ceramics were also prepared with solid state reaction method. Wherein, XRD measurements showed them to be pseudo-cubic phase. In the studies of composition-dependent structure of BF–BT binary solid solutions, the reported critical composition for structural phase boundary between rhombohedral and pseudocubic phase is very different, of which 0.725BF–0.275BT, 0.67BF–0.33BT, or a transition region between 0.25BT and 0.33BT has been reported till now [17–19, 22–24]. Referring to Figs. 1 and 2, combinational XRD and SEM measurements showed that larger microstructure grain size causes the BF69.6–BZT1.4–BT29 lattice structure become more rhombohedrally distorted. It should be noted that SEM observations on those MnO_2-doped BF67.5–BZT2.5–BT30 and BF69.58–BZT1.42–BT29 ceramics were performed on the surface of as-sintered ceramic pellets [28, 29]. As known, the microstructure of surface of as-sintered ceramic pellet is very different from the fracture-surface, of which the latter reflects the real situation of ceramic bulk microstructure. Analogously, there also lack

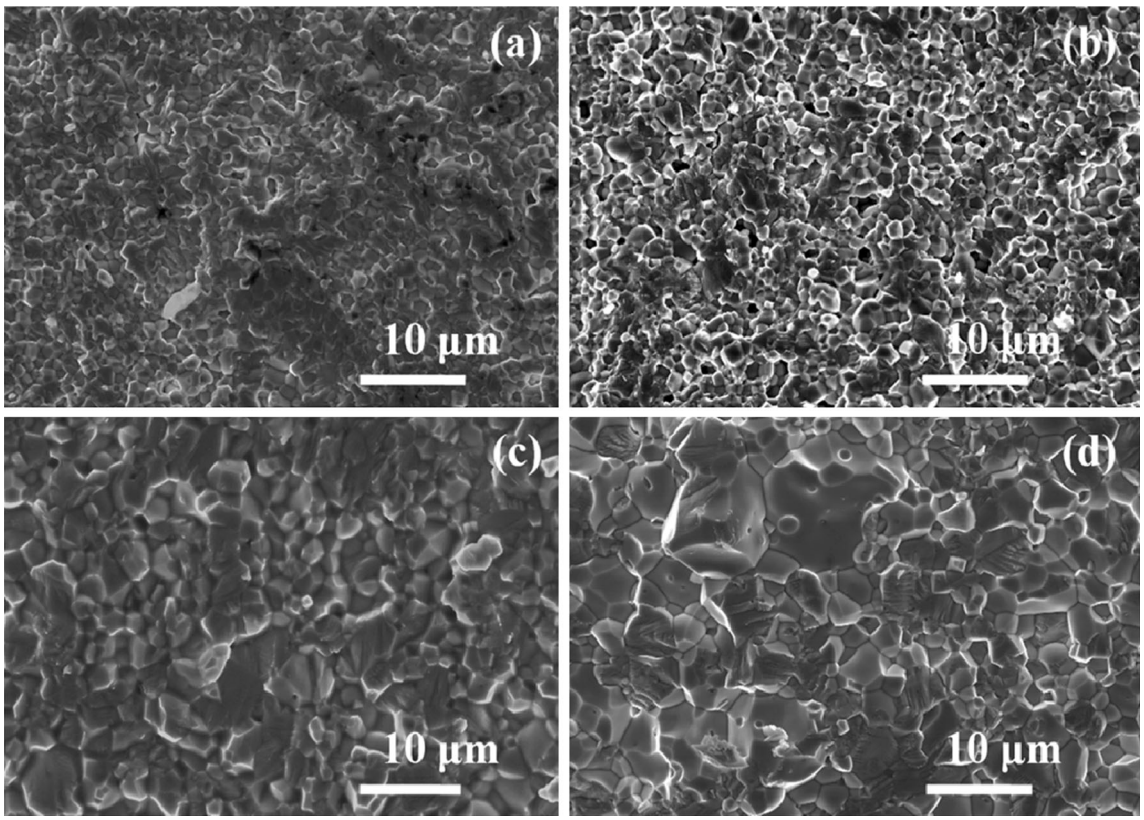

Fig. 2 SEM microstructure images observed on fracture surface for the **a** pure, **b** 0.20 %, **c** 0.22 %, and **d** 0.26 % in weight MnO_2-doped BF69.6–BZT1.4–BT29 ceramics

consistent XRD and SEM microstructure data on the BF–BT ceramics. Nevertheless, extensive studies on perovskite oxides revealed that microstructure grain size can set strong influence on the crystallographic structure and related composition-structural phase boundary position, which has been observed to induce lattice structural phase transition from low-symmetry to high-symmetry in nanocrystalline $BaTiO_3$ and $PbTiO_3$, or shifting of structural phase boundary position in fine-grained $Pb(Zr,Ti)O_3$, $0.8Pb(Mg_{1/3}Nb_{2/3})O_3$–$0.2PbTiO_3$ and $BiFeO_3$–$Bi(Zn_{1/2}Ti_{1/2})O_3$–$PbTiO_3$ (BF–BZT–PT) ceramics [26, 38–43]. From viewpoint of relationship between lattice structure and microstructure grain size of ceramics, the 0.67BF–0.33BT is reasonably believed as the critical composition of the rhombohedral-pseudocubic structural phase boundary for the coarse-grained BF–BT ceramics, which will shift towards BF-riched corner with decreasing microstructure grain size [30].

3.2 Dielectric properties

Usually Bi-perovskites exhibit large dielectric loss, which limit experimental characterizations of ferroelectric and piezoelectric properties. Like the case of BF–BZT–PT ternary solid solution [25, 26], adding BZT into BF–BT is expected to decrease dielectric loss and ease their electrical measurements. For the pure and various MnO_2-doped BF69.6–BZT1.4–BT29 ceramics sintered at 900 °C for 10 h, frequency dependent dielectric constant ε_r and loss $\tan\delta$ were measured at room temperature and presented in Fig. 3. From Fig. 3, it was seen that large dielectric loss of $\tan\delta$ more than 0.1 was observed in the undoped BF69.6–BZT1.4–BT29 ceramics. Taking the purity of used raw oxides into account, if the used raw oxides are all purified more than 99.9 %, it is treated as no A-site vacancies introduced in advance. Here, both Bi_2O_3 and $BaCO_3$ raw oxides used for preparation of BF69.6–BZT1.4–BT29 ceramics are low purity so that 0.73×1 % (Bi vacancies) + 0.27×0.2 % (Ba vacancies) = 0.784 % (A-site vacancies) were introduced in advance. Meanwhile, bismuth oxide usually evaporate during high temperature sintering so that the real concentration of A-site vacancies may be higher than the value calculated above [20, 21]. Owing to electric-neutrality, the charge compensation mechanism causes correspondingly same concentration of oxygen vacancies in the BF–BZT–BT ceramics [38–40]. Therefore, the large dielectric losses observed in the undoped BF69.6–BZT1.4–BT29 ceramics can be reasonably attributed to dielectric relaxation caused by a large

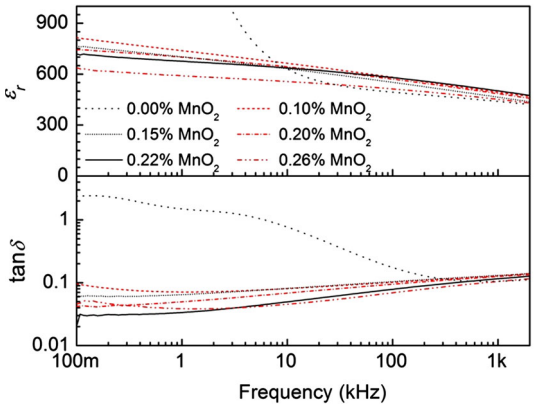

Fig. 3 Frequency dependent dielectric constant ε_r and loss tanδ measured at room temperature for various MnO_2-doped BF69.6–BZT1.4–BT29 ceramics

amount of space charges, charged A-site and O-site vacancies. Our extensive studies showed that this dielectric relaxation caused by space charge was still occurring when BZT content was increased to 5 %, but completely suppressed when BZT content was 10 % for those BF–BZT–BT ceramics with BF content more than 60 %. For example, tanδ = 0.022 was recorded at room temperature and frequency of 1 kHz in the BF75–BZT10–BT15 ceramics sintered at 900 °C for 10 h [30].

Contemporarily, as showed by Fig. 3, Mn-doping was observed effective to suppress this dielectric relaxation caused by space charge. In contrast to pure BF69.6–BZT1.4–BT29 ceramics, no dielectric relaxation was observed for those ceramics with MnO_2 addition more than 0.10 wt% performed here and the dielectric loss was all <0.14 over the frequency range of 100 Hz–2 MHz. For the 0.22 wt% MnO_2-doped sample, a minimum dielectric loss was obtained, of which the dielectric constant decreases while dielectric loss increases with increasing frequency. ε_r = 675 and tanδ = 0.033 was recorded for the 0.22 wt% MnO_2-doped BF69.6–BZT1.4–BT29 ceramics at room temperature and frequency of 1 kHz. It is known that Mn dopant can solid soluted into the perovskite lattice and prefers occupying on the B-site while its valance increases at higher sintering temperature. Owing to its varied valance and strong bonding with oxygen, doping Mn into BF–BZT–BT system will reduce remarkably the concentration of oxygen vacancies while increase slightly the concentration of A-site vacancies [1, 38, 39]. Therefore, doping MnO_2 decrease remarkably dielectric loss of BF–BZT–BT ceramics as showed in Fig. 3, the 0.22 wt% MnO_2-doped BF69.6–BZT1.4–BT29 ceramic sample exhibits the lowest concentration of vacancies in accordance with dielectric loss measurements. It is of interest to note that the optimal MnO_2 addition of 0.22 wt% obtained here is about 0.73 mol% MnO_2, which is very around the concentration of A-site vacancies introduced into ceramics in advance. Recently, a weak BZT composition dependence was observed with tanδ ~ 0.045 for the 1 mol% MnO_2-doped BF(70−x)–BZTx–BT30 (x = 0–15) ceramics sintered at 960 °C for 2 h [28]. For those BF–xBT ($0.25 < x \leq 0.33$) ceramics, large dielectric losses were reported with tan$\delta > 0.075$ for undoped ceramics [24] and tan$\delta > 0.06$ with 0.1 wt% MnO_2 dopant [22, 23]. So far, combined with those experimental observations on BF–BZT–PT, $Bi_{1-x}La_xFe_{1-y}Ti_yO_3$ and MnO_2-doped BF–BMT–BT ceramics [25–27, 30, 33], it is able to be concluded that to form ternary solid solution can stabilize greatly the $BiFeO_3$-based perovskite phase and thus reduce remarkably the Bi volatility, here low dielectric loss ceramics were obtained through adding BZT and Mn into BF–BT system combined with refined solid state reaction electroceramic processing. Those underlying mechanism needs more experiments and analyses in details.

For the 0.20, 0.22 and 0.26 wt% MnO_2-doped BF69.6–BZT1.4–BT29 ceramics, temperature-dependent dielectric properties were measured and the obtained results presented in Fig. 4. Determining from dielectric constant anomaly peak position showed in Fig. 4, ferroelectric phase transition temperature T_C at frequency of 1000 kHz was recorded as 518, 513, 514 °C , respectively, for the 0.20, 0.22 and 0.26 % MnO_2-dopant in weight. On the MnO_2-doping effect on T_C observed here, two opposite effects seem underlying there: T_C decreases with increasing Mn-doping amount (composition effect) while increases with increasing microstructure grain size (Mn-doping effect on kinetic behaviour of grain growth). It is of interest to note that doping MnO_2 into BF69.6–BZT1.4–BT29 ceramics not only decreases the room temperature dielectric loss but also those high temperature ones. It was seen from Fig. 4 that the dielectric loss of MnO_2-doped BF69.6–BZT1.4–BT29 ceramics decreases with increasing temperature from room temperature and the 0.22 wt% addition

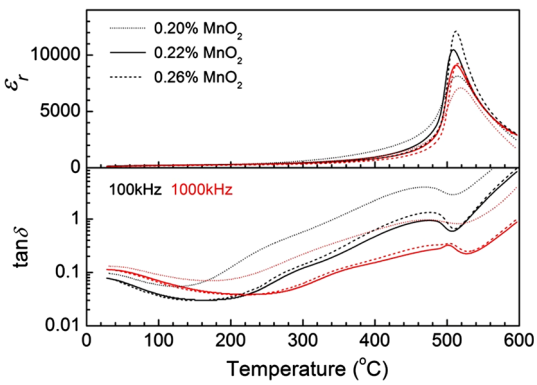

Fig. 4 Temperature dependence of dielectric constant ε_r and loss tanδ at the 100 and 1000 kHz frequency for 0.20, 0.22, and 0.26 % in weight MnO_2-doped BF69.6–BZT1.4–BT29 ceramics

is around optimal amount, which is substantial for time and thermal aging stabilities of piezoelectric performances.

Compared with the BF–BT binary system, ferroelectric T_C of the BF–BZT–BT ternary system was observed to decrease gradually with increasing BZT content when fixed BT content, $T_C = 583$, 559, and 529 °C was determined for the 1 mol% MnO_2-doped BF70–BT30, 1 mol% (~0.3 wt%) MnO_2-doped BF67.5–BZT2.5–BT30, and 1 mol% MnO_2-doped BF65–BZT5–BT30 ceramics, respectively [28]. In the 0.6 wt% MnO_2-doped $0.71(BF_{1-x}BZT_x)$–0.29BT ceramics, T_C was also observed to decrease gradually with increasing BZT content x up to 5 %, $T_C = 434$ and 425 °C was reported there for x = 0 (BF71–BT29) and x = 2 % (BF69.58–BZT1.42–BT29) ceramics [29]. Referring to the BF–xBT phase diagram, it is known that T_C in BF–BZT–BT system will decrease with increasing BT content [22], or increasing BZT content [28, 29], or increasing Mn dopant [22, 28, 29]. Moreover, extensive studies on 1 mol% MnO_2-doped BF65–BZT5–BT30 ceramics have also revealed T_C dependence on microstructure grain size. [28] So far, it is seen that ferroelectric T_C is closely associated with so many factors including composition, doping amount and microstructure grain size. As pointed out above in "Structural characterizations" section, there lack consistent observations on microstructure grain size and T_C for same composition and doping amount in BF–BZT–BT ternary system. Therefore, to interpret big discrepancy of T_C for similar compositions of 0.22 wt% MnO_2-doped BF69.6–BZT1.4–BT29 studied here, 1 mol% (~0.3 wt%) MnO_2-doped BF67.5–BZT2.5–BT30 [28], and 0.6 wt% MnO_2-doped BF69.58–BZT1.42–BT29 [29] ceramics needs more consistent experimental measurements and analyses.

3.3 Ferroelectric properties

P–E hysteresis loop measurements were carried out applying electric field of 120 kV/cm at frequency of 10 Hz to characterize ferroelectric properties of pure and Mn-doped BF69.6–BZT1.4–BT29 ceramics. For the undoped BF69.6–BZT1.4–BT29 ceramics, owing to larger dielectric losses as showed in Fig. 3, saturated P–E hysteresis loop was unavailable to be recorded. Here, we obtained saturated P–E hysteresis loops for the 0.15 ~ 0.26 wt% MnO_2-doped ceramics sintered at 900 °C for 10 h and 0.22 wt% MnO_2-doped ceramics sintered at 880 °C for 2 h and those results presented in Fig. 5. It was seen from Fig. 5 that the squareness of P–E hysteresis loop is closely dependent on the amount of Mn-dopant and sintering temperature. Remanent polarization $P_r = 18.7$ μC/cm^2 and coercive field $2E_c = 72$ kV/cm, $P_r = 22.6$ μC/cm^2 and $2E_c = 70$ kV/cm, $P_r = 25.4$ μC/cm^2 and $2E_c = 60$ kV/cm, $P_r = 25.1$ μC/cm^2 and $2E_c = 80$ kV/cm were recorded for the 0.15, 0.20, 0.22 and 0.26 wt% MnO_2-doped BF69.6–BZT1.4–BT29 ceramics sintered at 900 °C for 10 h, respectively. With lower sintering temperature, P_r was found decreased while E_c increased, $P_r = 12.7$ μC/cm^2 and $2E_c = 64$ kV/cm recorded for the 0.22 wt% MnO_2-doped ceramics sintered at 880 °C for 2 h. Combined with SEM observations showed in Fig. 2, the microstructure grain size increases monotonously with increasing MnO_2 dopant from 0.15 to 0.26 wt%. Previously, it is observed that decreasing microstructure grain size would cause a reduction of domain size and even transformation from multi-domain to single domain in $BaTiO_3$ and $Pb(Zr,Ti)O_3$ ferroelectric ceramics, which increases E_c accompanying with P_r decreasing in a monotonous way [41–43]. It is seen that only microstructure grain size effect could not interpret the abnormal increased E_c observed in the 0.26 wt% MnO_2-doped BF69.6–BZT1.4–BT29 ceramics studied here. Referring to dielectric loss measurements showed in Fig. 3, it was found that the variation of E_c with increasing MnO_2 addition exhibits same trend as dielectric loss, i.e. the smallest E_c was obtained in the sample with smallest tanδ, and that the variation of P_r with increasing MnO_2 addition exhibits opposite trend to dielectric loss, i.e. the largest P_r was obtained in the sample with smallest tanδ. Combined with microstructure grain size effect and point defect effect, an optimal concentration of A-site vacancies is interesting to obtain a maximum spontaneous and remanent polarization with minimum coercive field in the BF–BZT–BT coarse-grained ceramics. It is seen from Figs. 3 and 4 that 0.22 wt% MnO_2 is optimal amount not only for dielectric loss but also for ferroelectric properties of BF69.6–BZT1.4–BT29 ceramics studied here.

On the other hand, it was also found that both P_r and E_c increase monotonously with increasing applied electric field during P–E hysteresis loop measurements for all MnO_2-

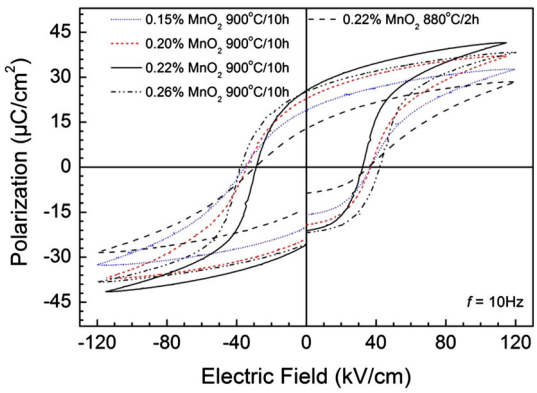

Fig. 5 P–E hysteresis loops measured applying 120 kV/cm electric field at room temperature and frequency of 10 Hz on the various Mn-doped BF69.6–BZT1.4–BT29 ceramics sintered at 900 °C for 10 h or 880 °C for 2 h

doped BF69.6–BZT1.4–BT29 ceramics. In the MnO_2-doped BF–BMT–BT ceramics, this trend of P_r increasing with increasing applied electric field was reported previously [33]. When applied electric field was 70 kV/cm, a saturated P–E hysteresis loop was obtained with $P_r = 21.4$ μC/cm^2 and $2E_c = 54$ kV/cm for the 0.22 wt% MnO_2-doped BF69.6–BZT1.4–BT29 ceramics sintered at 900 °C for 10 h. Previously, for 1 mol% MnO_2-doped BF67.5–BZT2.5–BT30 ceramics sintered at 960 °C for 2 h, its resistivity was measured more than 2×10^9 Ωcm under electric field of 30 kV/cm and a saturated P–E hysteresis loop was obtained under applied electric field of 70 kV/cm, of which $P_r = 23$ μC/cm^2 and $2E_c = 70$ kV/cm was recorded [28]. Similar case was observed in the 0.1 wt% MnO_2-doped BF69–BT31 ceramics with $P_r = 18.8$ μC/cm^2 and $2E_c = 46$ kV/cm [22]. So far, good ferroelectric polarization switching observed here is helpful to set full poling treatment for piezoelectricity.

3.4 Piezoelectric properties

For ferroelectric ceramics, poling treatment is required to align those randomly oriented grains and re-orient or switch domains to the applied field to set piezoelectricity. Customarily, a DC electric field more than $2E_c$ is required for full poling. In accordance with P–E hysteresis loop measurements showed in Fig. 5, poling treatment was carried out in silicon oil at 120 °C under electric field of 80 kV/cm for the BF69.6–BZT1.4–BT29 ceramics studied here and their piezoelectric constants were measured at room temperature after aging 24 h. Here, it was found that piezoresponse is strongly dependent on Mn-dopant amount and sintering temperature. Without Mn doping, the ceramics with large dielectric loss (referring to Fig. 3) is very much difficult to sustain high DC electric field even at room temperature for poling. Doping 0.10 wt% MnO_2 into BF69.6–BZT1.4–BT29 ceramics makes available poling at 30 °C under electric field of 66 kV/cm, then $d_{33} = 64$ pC/N was recorded. When MnO_2 dopant amount exceeds over 0.15 wt%, the poling was realized at 120 °C with DC electric field more than 80 kV/cm. Those obtained d_{33}, P_r, $\varepsilon_{33}^T/\varepsilon_0$, and tanδ for the low dielectric loss BF69.6–BZT1.4–BT29 ceramics with respect to MnO_2-dopant amount were summarized in Fig. 6. As demonstrated in Fig. 6, a maximum piezoresponse was obtained with MnO_2-dopant between 0.20 and 0.26 wt% for the BF69.6–BZT1.4–BT29 ceramics.

It is known that piezoelectric constant d_{33} is related to dielectric constant ε_{33} and induced polarization P_3 with the following relationship:

$$d_{33} = 2Q_{11}P_3\varepsilon_{33} \quad (1)$$

where Q_{11} is longitudinal electrostrictive coefficient and usually constant [1]. Therefore, larger dielectric constant and easier polarization switching (described by larger P_r and smaller E_c) are required to produce large piezoelectric constant. Combined with Figs. 5 and 6, it is seen that the maximum piezoelectric response observed in the MnO_2-doped BF69.6–BZT1.4–BT29 ceramics mainly comes from the easy spontaneous polarization switching. This observation is also proved by the data obtained in 0.22 wt% MnO_2-doped BF69.6–BZT1.4–BT29 ceramics sintered at 880 °C for 2 h, which just exhibits smaller $\varepsilon_r = 579$, $P_r = 12.7$ μC/cm^2 and then $d_{33} = 32$ pC/N smaller, correspondingly.

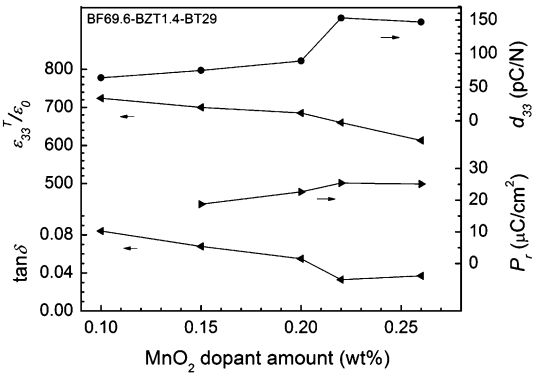

Fig. 6 Piezoelectric constant d_{33}, remanent polarization P_r, dielectric constant $\varepsilon_{33}^T/\varepsilon_0$ and loss tanδ for various Mn-doped BF69.6–BZT1.4–BT29 ceramics

In our experiments, an optimal piezoelectric property of $d_{33} = 150$ pC/N, $k_p = 0.36$, $k_t = 0.42$, $\varepsilon_{33}^T/\varepsilon_0 = 660$, tanδ = 0.033, and $T_C = 513$ °C was obtained in the 0.22 wt% MnO_2-doped BF69.6–BZT1.4–BT29 ceramics sintered at 900 °C for 10 h. In contrast, a good piezoelectric property of $d_{33} = 147$ pC/N, $k_p = 0.33$, $k_t = 0.43$, $\varepsilon_{33}^T/\varepsilon_0 = 613$, tanδ = 0.037, and $T_C = 514$ °C was obtained in the 0.26 wt% MnO_2-doped BF69.6–BZT1.4–BT29 ceramics sintered at 900 °C for 10 h. Those good piezoelectric properties obtained here for coarse-grained BF–BZT–BT ceramics were summarized in Table 1. For comparison, some data previously obtained in those ceramics of BF–BT binary system [17–19, 22–24], BF–BZT–BT ternary system [28, 29] and commercial piezoceramics including PZT-2 and PZT-6B [44], MLT [45], and BM901 [46] were also listed in Table 1. In the series of (0.70−x)BF–xBZT–0.30BT with x = 0–0.15, a maximum piezoresponse was obtained at x = 0.05 with piezoelectric property of $d_{33} = 139$ pC/N, $k_p = 0.31$, $\varepsilon_r = 650$, tanδ = 0.043, and $T_C = 529$ °C, summarized in Table 1 [28]. On one hand, compared with those BF–BT ceramics with compositions near the rhombohedral–pseudocubic structural phase boundary as showed in Table 1, adding BZT third end member is substantial to enhance piezoelectric performance of lead-free BF–BT ceramics taking advantage of extending structural phase boundary. On the other hand, in comparison with those commercial ferroelectric piezoceramics including both perovskite-type PZT-

Table 1 Summary of piezoelectric properties for BF-BZT-PT and BF-BT ferroelectric ceramics. Those for commercial PZT-2, PZT-6B, lead titanate (MLT) and lead metaniobate (BM901) ceramics are also presented for comparison

	$\varepsilon_{33}^{T}/\varepsilon_0$ (ε_r)	tanδ (tanδ)	d_{33} (pC/N)	T_C (°C)	k_t (k_p)	References
BF69.6−BZT1.4−BT29 + 0.22wt %MnO_2	660	0.033	150	513	0.42 (0.36)	This work
BF69.6−BZT1.4−BT29 + 0.26wt %MnO_2	613	0.037	147	514	0.43 (0.33)	This work
BF69.58−BZT1.42−BT29 + 0.6wt %MnO_2			163	425	(∼0.28)	[29]
BF65−BZT5−BT30 + 1at %MnO_2	(650)	(0.043)	139	529	(0.31)	[28]
BF75−BT25 + 0.1wt % MnO_2	(557)	(0.046)	116	619		[22, 23]
BF72.5−BT27.5	760	0.078	124		(0.29)	[24]
BF70−BT30	900	0.088	134	508	(0.29)	[18]
BF69−BT31 + 0.1wt % MnO_2	(704)	(0.067)	82	598		[22, 23]
BF67−BT33 + 0.1wt % MnO_2	(750)	(0.068)	70	605		[22, 23]
PZT−2	450	0.005	152	370	0.51 (0.47)	[44]
PZT−6B	460	0.009	71	∼350	0.30 (0.25)	[44]
MLT	170	0.008	51	495	0.46 (0.07)	[45]
BM901	325	0.01	90	490	0.40 (0.07)	[46]

2, PZT-6B, and MLT and tungsten bronze-type BM901, MnO_2-doped BF–BZT–BT ceramics exhibit better piezoelectric performance, due to higher dielectric constant, combined with higher Curie temperature.

By the end, time and temperature aging stabilities of piezoelectric constant d_{33} were measured for the 0.22 and 0.26 wt% MnO_2-doped BF69.6–BZT1.4–BT29 ceramics and the results presented in Fig. 7. For the 0.22 and 0.26 wt% MnO_2-doped ceramics, d_{33} = 167 and 152 pC/N was measured after poling treatment, respectively. After 1 day (24 h) aging, they became 157 and 147 pC/N while after 180 days (3 months) aging, they were measured as 141 and 140 pC/N, respectively. For 24 h aged samples, when they were heat treated at 100 °C for 10 min and then cooled to room temperature, d_{33} = 145 and 143 pC/N was measured for the 0.22 and 0.26 wt% MnO_2-doped ceramics, respectively. As showed in Fig. 7, d_{33} decreases slightly for both samples till thermal-aging temperature gradually increasing up to 400 °C, and then decreases remarkably when aging temperature more than 400 °C. Therefore, it is concluded that the 0.22 and 0.26 wt% MnO_2-doped BF69.6–BZT1.4–BT29 ceramics studied here exhibit excellent time and thermal aging stabilities of piezoelectric constant. This temperature-aging observation is in agreement with previous report by Shan, et al., on 0.6 wt% MnO_2-doped 0.71($BF_{1-x}BZT_x$)–0.29BT ceramics with $x \leq 3$ % [29]. Similar depolarization temperature ($T_d \sim 400$ °C) was obtained here, which is consistent with that as expected in BF–BT and related piezoceramics [4]. As known, for those extensive studied lead-free piezoceramics of $K_{1-x}Na_xNbO_3$ and (1−x)($Bi_{0.5}Na_{0.5}$)TiO_3–x$BaTiO_3$ with composition at structural phase boundary, their ferroelectric T_C are 420 and 288 °C while there occurs

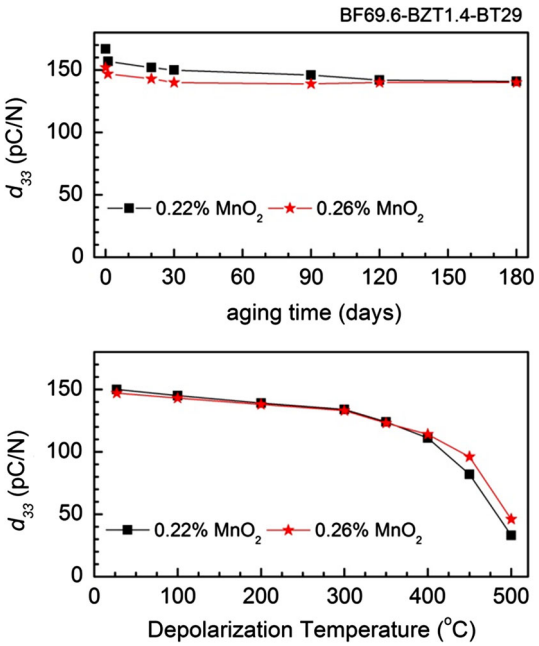

Fig. 7 Piezoelectric constant d_{33} measured with various time aging and depolarization temperature heat-treatment for the 0.22 and 0.26 % in weight MnO_2-doped BF69.6–BZT1.4–BT29 ceramics

one FE–FE structural phase transition at 195 and 105 °C, respectively. This FE–FE structural phase transition sets strong influence on thermal aging stability of their piezoelectric properties [2, 4]. Particularly, for recent up-rising star of (1−x)$Ba(Zr_{0.2}Ti_{0.8})O_3$–x$(Ba_{0.7}Ca_{0.3})TiO_3$ piezoceramics, their ferroelectric T_C are below 120 °C and the FE–FE transition temperature for 0.5$Ba(Zr_{0.2}Ti_{0.8})O_3$–0.5$(Ba_{0.7}Ca_{0.3})TiO_3$ is unfortunately around room temperature, which results in larger d_{33} of 580 ∼ 620 pC/N but

very poor thermal aging stability [7–9]. In contrast, both BF–BT and BF–BZT–BT systems with compositions near the rhombohedral–pseudocubic structural phase boundary has higher T_C more than 500 °C and no FE–FE phase transition below T_C. Therefore, excellent time and thermal aging stabilities of piezoelectric property of BF–BZT–BT ceramics showed in Fig. 7 can be well understood by their features of higher T_C more than 500 °C and no FE–FE phase transition below T_C. BF–BZT–BT is one promising candidate for future lead-free applications or high temperature applications because BZT-extended structural phase boundary provides big space to adjust piezoelectric performance and related time and temperature aging stabilities by changing composition.

4 Summary

Pure and MnO_2-doped BF69.6–BZT1.4–BT29 ceramics were prepared using a refined solid state reaction electroceramic processing and their structural and electrical properties were experimentally investigated. Compared with the BF–BT ceramics, it was found that both adding BZT third member and doping Mn remarkably decrease dielectric losses of BF–BZT–BT ceramics within refined solid state reaction electroceramic processing and realize to sustain high DC electric field at high temperature for poling. Their ferroelectric and piezoelectric properties were found dependent on Mn dopant amount and sintering temperature, a maximum piezoelectric and ferroelectric property was obtained in optimal 0.22 wt% MnO_2-doped BF69.6–BZT1.4–BT29 coarse-grained ceramics sintered at 900 °C for 10 h here. Excellent time and thermal aging stabilities of piezoelectric constant d_{33} were experimentally demonstrated and argued resulting from the features of higher T_C and no FE–FE structural phase transitions below T_C of BF–BZT–BT system.

Acknowledgments This work was partially supported by FANEDD-200744, NCET-07-0624, Shanghai Eastern Scholarship Program, and the Fundamental Research Funds for the Central Universities.

References

1. G.H. Haertling, J. Am. Ceram. Soc. **82**, 797 (1999)
2. J. Rödel, W. Jo, K.T.P. Seifert, E.M. Anton, T. Granzow, D. Damjanovic, J. Am. Ceram. Soc. **92**, 1153 (2005)
3. T. Shrout, S.J. Zhang, J. Electroceram. **19**, 113 (2007)
4. S.O. Leontsev, R.E. Eitel, Sci. Technol. Adv. Mater. **11**, 044302 (2010)
5. Y. Saito, H. Takao, T. Tani, T. Nonoyama, K. Takatori, T. Homma, T. Nagaya, M. Nakamura, Nature **432**, 84 (2004)
6. T. Takenaka, K. Maruyama, K. Sakata, Jpn. J. Appl. Phys. **30**, 2236 (1991)
7. W. Liu, X.B. Ren, Phys. Rev. Lett. **103**, 257602 (2009)
8. L. Zhang, M. Zhang, L. Wang, C. Zhou, Z. Zhang, Y.G. Yao, L.X. Zhang, D.Z. Xue, X.J. Lou, X.B. Ren, Appl. Phys. Lett. **105**, 162908 (2014)
9. H.X. Bao, C. Zhou, D.Z. Xue, J.H. Gao, X.B. Ren, J. Phys. D Appl. Phys. **43**, 465401 (2010)
10. B. Jaffe, W.R. Cook, H. Jaffe, *Piezoelectric ceramics* (Academic Press, London, 1971)
11. B. Noheda, D.E. Cox, G. Shirane, J.A. Gonzalo, L.E. Cross, S.E. Park, Appl. Phys. Lett. **74**, 2059 (1999)
12. R. Guo, L.E. Cross, S.E. Park, B. Noheda, D.E. Cox, G. Shirane, Phys. Rev. Lett. **84**, 5423 (2000)
13. R.E. Eitel, C.A. Randall, T.R. Shrout, P.W. Rehrig, W. Hackenberger, S.E. Park, Jpn. J. Appl. Phys. **40**, 5999 (2001)
14. T. R. Shrout, S. J. Zhang, R. Eitel, C. Stringer, and C. A. Randall, *IEEE Int. Ultrason. Ferroelect. and Freq. Control Joint 50th Ann. Conf.* 126 (2004)
15. I. Sterianou, D.C. Sinclair, I.M. Reaney, T.P. Comyn, A.J. Bell, J. Appl. Phys. **106**, 084107 (2009)
16. S. Wada, K. Yamato, P. Pulpan, N. Kumada, B.Y. Lee, T. Iijima, C. Moriyoshi, Y. Kuroiwa, J. Appl. Phys. **108**, 094114 (2010)
17. M.M. Kumar, A. Srinivas, S.V. Suryanarayana, J. Appl. Phys. **87**, 855 (2000)
18. Y.X. Wei, X.T. Wang, J.T. Zhu, X.L. Wang, J.J. Jia, J. Am. Ceram. Soc. **96**, 3163 (2013)
19. X.Z. Guo, Y.G. Wu, Y.N. Zou, Z.Y. Wang, J. Mater. Sci.: Mater. Electron. **23**, 1072 (2012)
20. J. Yu, J. Chu, Chi. Sci. Bull. **53**, 2097 (2008)
21. T. Rojac, A. Bencan, B. Malic, G. Tutuncu, J.L. Jones, J.E. Daniels, D. Damjanovic, J. Am. Ceram. Soc. **97**, 1993 (2014)
22. S.O. Leontsev, R.E. Eitel, J. Am. Ceram. Soc. **92**, 2957 (2009)
23. S.O. Leontsev, R.E. Eitel, J. Mater. Res. **26**, 9 (2011)
24. S.C. Yang, A. Kumar, V. Petkov, S. Priya, J. Appl. Phys. **113**, 144101 (2013)
25. X.B. Hou, J. Yu, J. Am. Ceram. Soc. **96**, 2218 (2013)
26. X.B. Hou, J. Yu, Jpn. J. Appl. Phys. **52**, 061501 (2013)
27. L.L. Zhang, J. Yu, M. Itoh, J. Appl. Phys. **115**, 123523 (2014)
28. Q.J. Zheng, Y.Q. Guo, F.Y. Lei, X.C. Wu, D.M. Lin, J. Mater. Sci.: Mater. Electron. **25**, 2638 (2014)
29. X. Shan, C.R. Zhou, Z.Y. Cen, H.B. Yang, Q. Zhou, W.Z. Li, Ceram. Int. **39**, 6707 (2013)
30. Y. Lin, L.L. Zhang, W.L. Zheng, J. Yu, J. Mater. Sci. Mater. Electron. (2015). doi:10.1007/s10854-015-3364-x
31. I. Fujii, R. Mitsui, K. Nakashima, N. Kumada, M. Shimada, T. Watanabe, J. Hayashi, H. Yabuta, M. Kubota, T. Fukui, S. Wada, Jpn. J. Appl. Phys. **50**, 09ND07 (2011)
32. C.R. Zhou, A. Feteira, X. Shan, H.B. Yang, Q. Zhou, J. Chen, W.Z. Li, H. Wang, Appl. Phys. Lett. **101**, 032901 (2012)
33. Y. Lin, J. Yu, J. Mater. Sci.: Mater. Electron. **25**, 5462 (2014)
34. Q. Zhou, C.R. Zhou, H.B. Yang, G.H. Chen, W.Z. Li, H. Wang, J. Am. Ceram. Soc. **95**, 3889 (2012)
35. K.Y. Yoon, H.K. Lee, H.R. Lee, J. Am. Ceram. Soc. **85**, 2753 (2002)
36. Y.D. Hou, M.K. Zhu, F. Gao, H. Wang, B. Wang, H. Yan, C.S. Tian, J. Am. Ceram. Soc. **87**, 847 (2002)
37. X.H. Liu, Z. Xu, S.B. Qu, X.Y. Wei, J.L. Chen, Ceram. Int. **34**, 797 (2008)
38. N.G. Eror, U. Balachandran, J. Solid Stat. Chem. **40**, 85 (1981)
39. L. Wang, Y. Sakka, Y. Shao, G.A. Botton, T. Kolodiazhnyi, J. Am. Ceram. Soc. **93**, 2903 (2010)
40. Z.Y. Shen, Q.G. Hu, Y.M. Li, Z.M. Wang, W.Q. Luo, Y. Hong, Z.X. Xie, R.H. Liao, J. Mater. Sci. Mater. Electron. **24**, 3089 (2013)

41. H.I. Hsiang, F.S. Yen, J. Am. Ceram. Soc. **79**, 1053 (1996)
42. C.A. Randall, N.C. Kim, J.P. Kucera, W.W. Cao, T.R. Shrout, J. Am. Ceram. Soc. **81**, 677 (1998)
43. T.M. Kamel, G. de With, J. Euro. Ceram. Soc. **28**, 851 (2008)
44. D. Berlincourt, Piezoelectric Crystals and Ceramics, in *Ultrasonic Transducer Materials*, ed. O. E. Mattiat (Plenum Press, New York, 1971) p. 63
45. T. Tanaka, K. Okazaki, N. Ichinose, *Piezoelectric Ceramic Materials* (Gakken-sha, Tokyo, 1973), p. 115 (**in Chinese**)
46. Sensor Technology Limited, BM901-Lead Metaniobate. http://www.sensortech.ca/userfiles/file/BM901.pdf